

# High-temperature oxidation behavior of a cast Ti-47.5Al-2.5V-1.0Cr-0.2Zr alloy

Xue-jian Lin, \*Hong-jun Huang, Xiao-guang Yuan, Yin-xiao Wang, Bo-wen Zheng, Xiao-jiao Zuo, and Ge Zhou

School of Materials Science and Engineering, Shenyang University of Technology, Shenyang 110870, China

**Abstract:** The oxidation behavior of the Ti-47.5Al-2.5V-1.0Cr-0.2Zr alloy at 900 °C was investigated at different oxidation times (5, 20, 60 and 100 h). The results show that the total weight gain of the alloy after 100 h at 900 °C oxidation is 9.1 g·m<sup>-2</sup>, and the oxidation rate decreases with oxidation time. The oxides on the alloy surface are mainly TiO<sub>2</sub> and Al<sub>2</sub>O<sub>3</sub>. At the beginning of oxidation (5 h), the oxide film is relatively complete, thin, and the interface between the oxide layer and the matrix is virtually flat. At the end of oxidation (100 h), the thickness of the oxide film is expanded, cracking and spalling occur, and the spalling form is intra-film spalling. At the same time, oxygen is mainly distributed in the oxide film and the oxygen content in the alloy substrate is reduced, confirming that the TiAl alloy has a certain oxidation stability at 900 °C. From the outer surface of the oxide layer to the matrix, the TiO<sub>2</sub> content increases and the Al<sub>2</sub>O<sub>3</sub> content decreases. Oxidation proceeds to completion in this system via the dissolution and diffusion of O atom.

**Keywords:** cast TiAl alloy; high temperature oxidation; oxidation film; oxidation behavior

CLC numbers: TG146.23

Document code: A

Article ID: 1672-6421(2022)05-443-12

## 1 Introduction

TiAl alloys have the advantageous properties of high specific strength, high specific stiffness, and excellent oxidation resistance, which have been utilized for turbine blades in aircraft engines and automobile engines [1-3]. The blades are used in high-temperature conditions, with oxidation resistance being one of the important indices in determining its application potential. TiAl alloys can exhibit good oxidation resistance after long-term thermal exposure at 700 °C [4]. But, when the temperature exceeds 800 °C, the continuous and dense Al<sub>2</sub>O<sub>3</sub> protective oxide film cannot be generated on the surface, and instead a mixed oxide consisting of TiO<sub>2</sub> and Al<sub>2</sub>O<sub>3</sub> is formed. TiO<sub>2</sub> has a loose structure and large oxygen permeability, which cannot prevent the diffusion of O atoms, resulting in insufficient oxidation resistance; thus, restricting their further application [5-8]. Therefore, enhancing the oxidation resistance of TiAl alloys above 800 °C has become an urgent problem [9]. Domestic and foreign scholars have obtained results regarding the oxidation resistance of TiAl alloys [10, 11]. Studies

have shown that the addition of alloying elements containing Nb, Cr, Mo, W, and the rare earth element Y could promote the oxidation resistance of TiAl by inhibiting the growth of the less-desirable TiO<sub>2</sub> [14]. Liu et al. [15] observed that adding a small amount of Zr could slightly reduce the oxidation rate of the alloy and improve its oxidation resistance. Dade et al. [16] found that the addition of Zr improved the oxidation resistance of a Ti<sub>2</sub>AlNb alloy and did not result in the formation of a brittle phase. Meanwhile, the corresponding microstructure of the alloy has a great effect on its oxidation performance [17-19]. The oxidation kinetics of TiAl alloys with identical composition but different microstructures were studied by Gil et al. [20], proving refined TiAl alloy microstructure could enhance the spalling resistance of the oxide film. Surface treatments, including metal coatings such as Al-Si [21], Al-Nb [22], and Ti-Al-Cr [23, 24], and ceramic coatings, such as Al<sub>2</sub>O<sub>3</sub> [25], SiO<sub>2</sub> [26], and TiN [27], can also improve oxidation resistance by inhibiting oxygen diffusion into the interior matrix, which inhibits the rapid growth of TiO<sub>2</sub>. In summary, the oxidation behavior of TiAl alloys depends on the alloy's composition, microstructure, and surface treatment, among other factors [15, 17, 28]. These factors all affect the oxidation resistance, however, no systematic studies have been carried out in terms of oxidation kinetics, spalling form and delamination characteristics of oxide film.

### \*Hong-jun Huang

Male, Ph. D, Professor. His research interests mainly focus on composition design and forming technologies of aluminum and titanium aluminum alloys.

E-mail: huanghong1977@163.com

Received: 2022-05-17; Accepted: 2022-08-28

Studies into the oxidation of TiAl alloys are helpful in understanding the oxidation resistance of the alloy, and, at the same time, suitable means of oxidation resistance can be found according to the oxidation degree of the alloy during the oxidation process [10-12]. Therefore, further research regarding the oxidation behavior of the TiAl alloy becomes more urgent. The cast Ti-47.5Al-2.5V-1.0Cr-0.2Zr (at.%) alloy with a directional lamellar microstructure, under loading along the lamellar interface direction, shows good tensile strength and plastic combination at room temperature, and good mechanical properties at high temperatures (750–800 °C) [13]. However, research on the oxidation resistance of this alloy above 850 °C is still absent, and both the crack mechanism and the exfoliation form of the oxide film are not fully understood. Therefore, in this work, the oxidation kinetics, phase constitution, oxidized surface, and cross-sectional morphology of the oxide layer of the alloy at 900 °C and at different oxidation times were all characterized in detail, providing a theoretical and experimental basis for the analysis of this alloy's oxidation mechanism.

## 2 Experimental materials and methods

The matrix was a  $\gamma$ -TiAl alloy with nominal composition Ti-47.5Al-2.5V-1.0Cr-0.2Zr (at.%), hereinafter referred to as "TiAl alloy". The master alloy was obtained by remelting twice in a vacuum induction levitation furnace, then cast into a fixed die with the size of  $\Phi 40$  mm $\times$ 220 mm. The isothermal oxidation experiment on the TiAl alloy with lamellar microstructure was carried out at 900 °C. The oxidation sample was 10 mm $\times$ 10 mm $\times$ 5 mm in size, and was placed in a thermogravimetric crucible in the form of point contact. A thermogravimetric crucible with size of  $\Phi 20$  mm $\times$ 12 mm, burned to a constant weight, was used in the experiment. The oxidation test was carried out at 900 °C for 5, 20, 60, and 100 h. Weight measurement of samples at different oxidation stages was conducted using an analytical balance with a accuracy of 0.01 mg. The microstructure, composition distribution and phase constitution of the oxidized samples were analyzed using scanning electron microscopy (SEM), laser confocal microscopy, energy dispersive spectroscopy (EDS), X-ray photoelectron spectroscopy (XPS), and X-ray diffraction (XRD).

## 3 Results and discussion

### 3.1 Oxidation kinetics of TiAl alloy

#### 3.1.1 Oxidation kinetics curve

The oxidation kinetics curve of the TiAl alloy at 900 °C for 100 h (Fig. 1) indicates that the TiAl alloy experiences two stages during high-temperature oxidation: rapid weight gain, and slow weight gain. The oxidation kinetics curve approximately obeys a parabolic growth law, indicating that the oxidation process is greatly dependent on the diffusion of metal ions and oxygen in the oxide film [29]. It is also

observed that the total weight gain of the alloy after 100 h oxidation is 9.1 g·m<sup>-2</sup>. Zhao et al. [30] found that the oxidation weight gain per unit area of Ti45Al8Nb, Ti45Al8Nb0.6Y and Ti45Al8Nb0.1Y alloys after oxidation at 900 °C/100 h was 10.1 g·m<sup>-2</sup>, 14.2 g·m<sup>-2</sup>, and 13.1 g·m<sup>-2</sup>, respectively; therefore, the alloy studied in this study has better oxidation resistance.

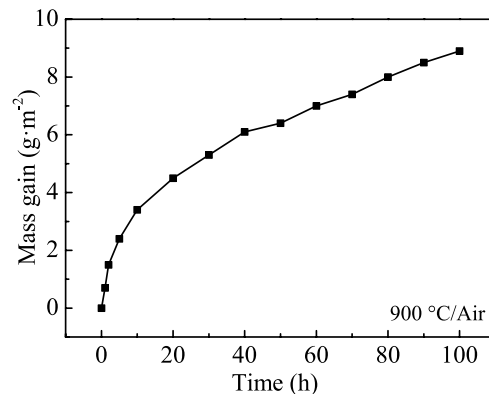


Fig. 1: Oxidation kinetics curve of TiAl alloy at 900 °C

#### 3.1.2 Oxidation kinetics equation

The oxidation rate of the alloy during oxidation can be expressed as Eq. (1):

$$\Delta w^n = k_p t \quad (1)$$

where  $\Delta w$  is the oxidation weight gain (g·m<sup>-2</sup>) during the oxidation process;  $n$  is a power-exponential constant;  $k_p$  is the oxidation rate constant (g<sup>n</sup>·m<sup>-2n</sup>·s<sup>-1</sup>); and  $t$  is oxidation time (h). Taking logarithms of both sides of Eq. (1), the Eq. (2) was obtained:

$$n \ln \Delta w = \ln k_p + \ln t \quad (2)$$

According to the oxidation kinetics data, the  $\ln \Delta w - \ln t$  curve has a linear fit, as shown in Fig. 2. The power-exponent constant  $n$  and oxidation rate constant  $k_p$  of the TiAl alloy at different stages are shown in Table 1.

It can be seen that the value of  $n$  corresponding to the initial oxidation (0–10 h) of the TiAl alloy is small (1.96), indicating that the rate of variation in oxidation weight gain per unit area of the alloy with oxidation time is between linear and parabolic. In this process, the oxidation rate is faster, and the oxide is generated rapidly. The value of  $n$  corresponding to the medium-term oxidation (10–40 h) of the alloy increases to 2.38, indicating that the oxidation rate is decreased at this time; a protective continuous oxide film is formed, thereby slowing down further oxidation. The  $n$  value during the late oxidation (40–100 h) of the TiAl alloy is further increased to 2.49; that is, the oxidation rate slows down. To summarize, the constant value of oxidation rate of the alloy increases with the increase of oxidation time.

### 3.2 Constitution and morphology of oxide film

#### 3.2.1 Phase constitution

The constitution of the products from surface oxidation of the TiAl alloy after different oxidation times at 900 °C was

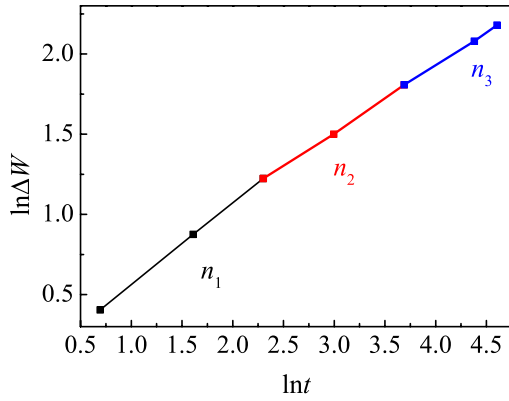


Fig. 2: Relationship between oxidation weight gain and time

Table 1: Change of power-exponential constant ( $n$ ) and oxidation rate constant ( $k_p$ ) with oxidation time

Time	$n$	$k_p$	Oxidation kinetics law
0–10 h	1.96	1.107	$\Delta w = (1.107t)^{0.51}$
10–40 h	2.38	1.817	$\Delta w = (1.817t)^{0.42}$
40–100 h	2.49	2.211	$\Delta w = (2.211t)^{0.40}$

analyzed via XRD (Fig. 3). Results indicate that the oxides are mainly  $\text{TiO}_2$  and  $\text{Al}_2\text{O}_3$  after different oxidation times. The  $\text{TiO}_2$  diffraction peak intensity is clearly higher than that of  $\text{Al}_2\text{O}_3$ , indicating the  $\text{TiO}_2$  content is higher and increases with oxidation time, but the change in  $\text{Al}_2\text{O}_3$  content over time is unclear. The thermodynamic data show that the difference in free energy between  $\text{TiO}_2$  and  $\text{Al}_2\text{O}_3$  is small [31]. During the initial oxidation, Ti and Al are oxidized. However, due to the high oxygen partial pressure at the surface, TiO is rapidly oxidized to  $\text{TiO}_2$ , and the diffusion rate of Ti is fast. Therefore, the alloy's surface following long-term oxidation is mainly consisted of  $\text{TiO}_2$  [32].

Figure 4 shows the relationship between the oxidation rate constants of  $\text{TiO}_2$  and  $\text{Al}_2\text{O}_3$  with temperature [33]. It can be seen that the growth rate of  $\text{TiO}_2$  is significantly faster than that of  $\text{Al}_2\text{O}_3$  at the same temperature, and the rapid growth of  $\text{TiO}_2$  is the main reason for the poor oxidation resistance of the alloy. In addition to oxides, the diffraction peaks of the matrix phase ( $\gamma\text{-TiAl}$  and  $\alpha\text{-Ti}_3\text{Al}$ ) are also detected, and  $\gamma\text{-TiAl}$  phase is shown to be the main phase (Fig. 3). The  $\beta/\text{B2}$  phase is also included in the TiAl alloy, but due to its low content and the presence of the oxidized film, the corresponding diffraction peak intensity is low, so this phase is not marked. The presence of the matrix phase may be due to two reasons: the X-ray penetrates the thin oxide layer and diffracts to the matrix, and the oxide layer on the alloy surface is incomplete.

### 3.2.2 Morphology

Figures 5 and 6 show the two- and three-dimensional morphologies of the sample surface after different oxidation times using laser confocal microscopy. It can be seen that after

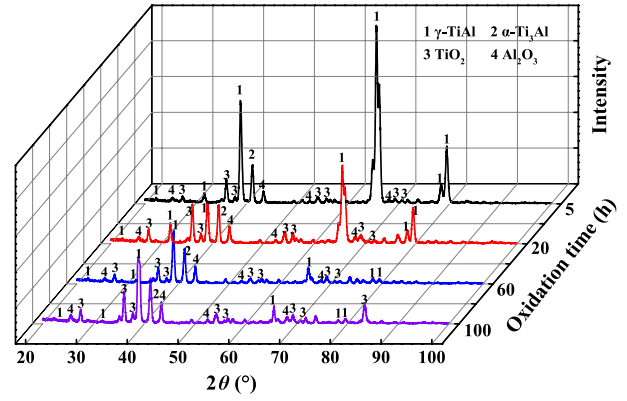


Fig. 3: XRD patterns of oxidation of TiAl alloy after oxidation test at 900 °C

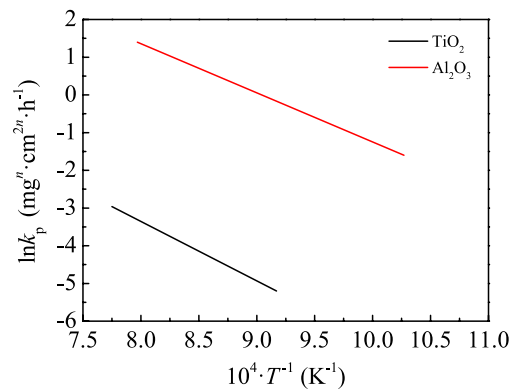


Fig. 4: Relationship between oxidation rate constants and temperature

5 h oxidation, there are still scratches on the surface of the alloy. After 20 h oxidation, some oxide particles are observed, but these particles do not cover the scratches completely. After 100 h oxidation, the scratches on the surface of the sample are completely covered by oxide particles, and the oxide particles are more obvious and show uneven surfaces. The change in surface roughness of the sample after different oxidation times is shown in Fig. 7. As the oxidation process continues, the oxide grows further at the notch, resulting in a gradual increase in roughness. In the later stage of oxidation, due to the uneven size of the oxide particles, the surface roughness increases sharply.

Figure 8 shows SEM images of the TiAl alloy surface after treatment at 900 °C for different oxidation times. The surface oxide shows crystalline particles. During early oxidation (5 h), the number and volume of oxide particles are small, and scratches on the surface can be clearly observed. When the oxidation time increases to 20 h, the number of oxide particles increases, oxide agglomeration appears. In the middle stage of oxidation (60 h), a granular oxide gradually forms, the oxide agglomeration is more obvious, and the scratches still exist. After an oxidation time of 100 h, the scratches on the surface are mostly covered by oxide particles, and the size of the oxide agglomeration is large. In order to determine the composition of these oxides, EDS analysis was carried out, and the results are shown in Fig. 9. The granular oxide is a mixed oxide of  $\text{TiO}_2$  and  $\text{Al}_2\text{O}_3$ , and the  $\text{TiO}_2$  content is higher, which is

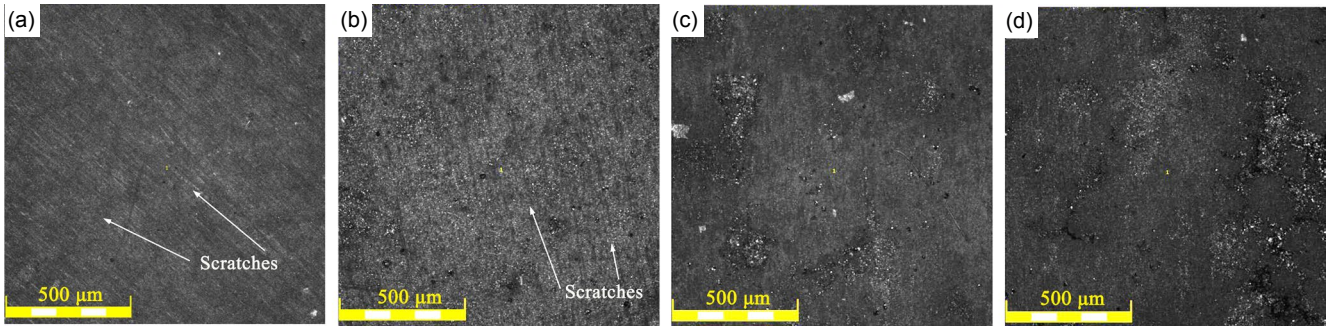


Fig. 5: Two-dimensional morphologies of sample surface: (a) 5 h; (b) 20 h; (c) 60 h; (d) 100 h

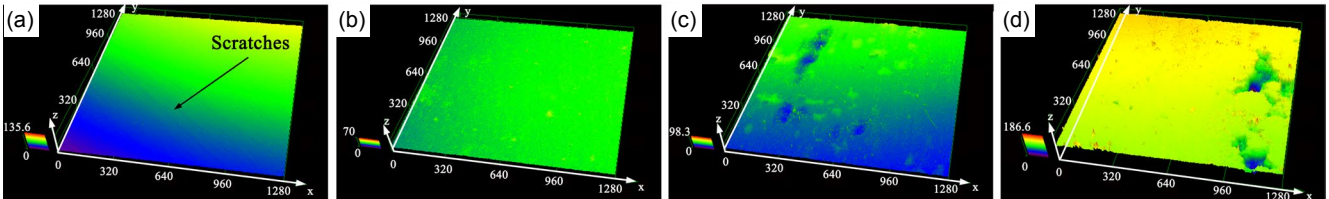


Fig. 6: Three-dimensional morphologies of sample surface: (a) 5 h; (b) 20 h; (c) 60 h; (d) 100 h

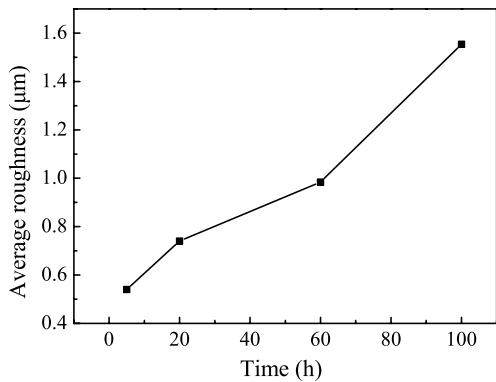


Fig. 7: Change of surface roughness of the sample

consistent with the XRD results. In summary, when the TiAl alloy is oxidized at 900 °C for different times, granular oxides composed of TiO<sub>2</sub> and Al<sub>2</sub>O<sub>3</sub> are formed. With extended oxidation times, the structural compactness of the oxides on the surface of the alloy changes, and the TiO<sub>2</sub> and Al<sub>2</sub>O<sub>3</sub> oxides gradually grow and increase in content.

### 3.2.3 Cross-sectional analysis

#### 3.2.3.1 Morphology

Figure 10 shows the cross-sectional morphology of the TiAl alloy after oxidation at 900 °C for different oxidation times. When the oxidation time is 5 h, the morphology of the oxide film is relatively complete and the thickness is small. When the oxidation time is 20 h, the thickness of the oxide film increases. As the oxidation time increases to 60 h, the thickness of the oxide film increases significantly, and the interface becomes curved. At the same time, holes can be observed, and these holes deteriorate the integrity of the oxide film. After 100 h oxidation, the cracking and spalling of the oxide film can be observed. The cracking and spalling of the oxide film are mainly due to the mismatch of thermal expansion coefficients between the oxide film and the matrix during heating and cooling. The thermal expansion coefficients of TiO<sub>2</sub>, Al<sub>2</sub>O<sub>3</sub> and TiAl alloy are  $8.2 \times 10^{-6} \text{ K}^{-1}$  [34],  $8.1 \times 10^{-6} \text{ K}^{-1}$  [35], and  $12.5 \times 10^{-6} \text{ K}^{-1}$  [13], respectively. A schematic diagram of cracking is shown in Fig. 11. During the heating period, the

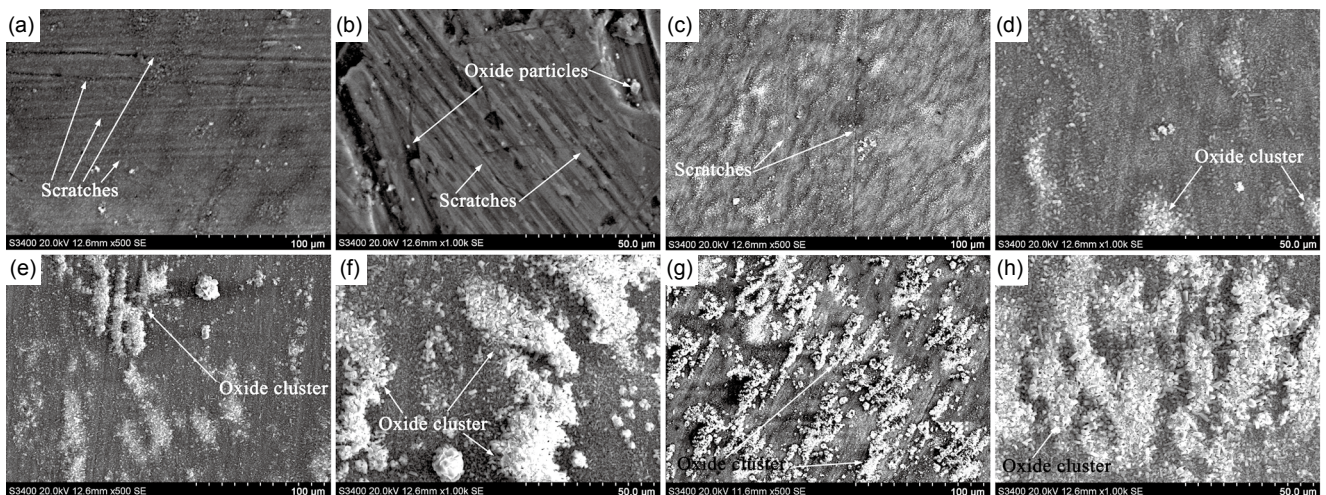


Fig. 8: SEM images of surface of TiAl alloy at 900 °C: (a, b) 5 h; (c, d) 20 h; (e, f) 60 h; (g, h) 100 h

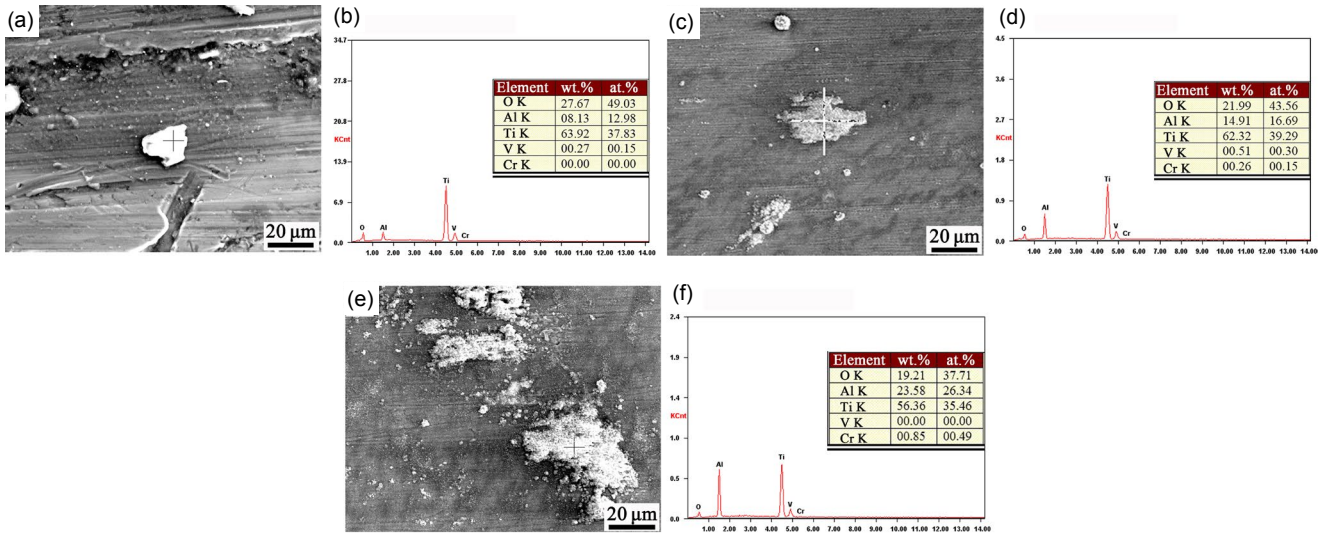


Fig. 9: EDS analysis of surface of TiAl alloy at 900 °C: (a, b) 5 h; (c, d) 20 h; (e, f) 60 h

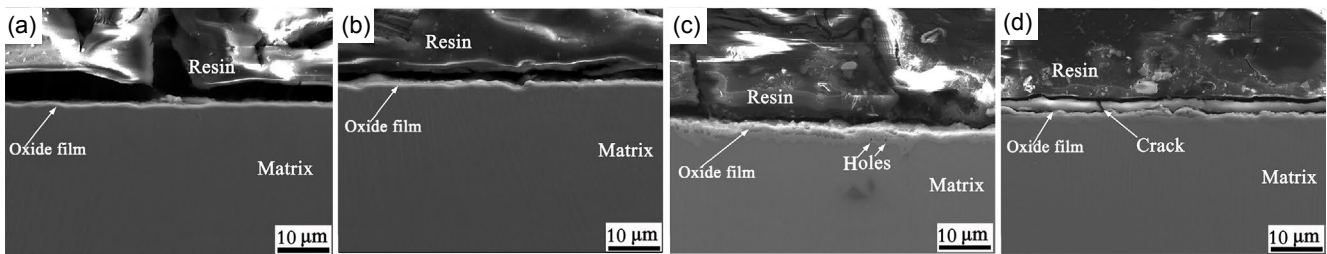


Fig. 10: Cross-sectional morphology of TiAl alloy at 900 °C: (a) 5 h; (b) 20 h; (c) 60 h; (d) 100 h

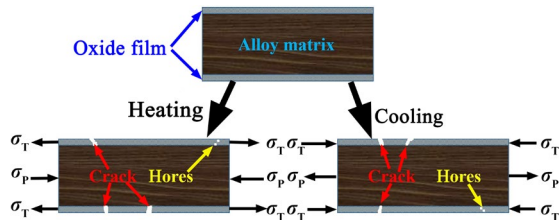


Fig. 11: Crack schematic diagram of TiAl alloy:  $\sigma_p$  (pressure stress);  $\sigma_t$  (tensile stress)

oxide film formed is subjected to the tensile stress ( $\sigma_t$ ) of the matrix; however, the matrix is subjected to the compressive stress ( $\sigma_p$ ) of the oxide film. The opposite is true during the cooling period. When the stress exceeds the critical cracking stress, the oxide film will crack or strip. At the same time, as the oxidation progresses, the size of the oxide particles ( $\text{TiO}_2$  and  $\text{Al}_2\text{O}_3$ ) increases significantly, reducing the binding force of the oxide film. Moreover, the increase in oxide film thickness increases the likelihood of exfoliation failure.

After oxidation at 900 °C for 100 h, the surface oxide film shows deformation, wrinkling, fracture, and even spalling. Large-scale spalling of the oxide film is the primary cause for the sharp decline in high-temperature oxidation performance of the TiAl alloy. For the TiAl alloy, the internal diffusion of O atoms and the external diffusion of metal ions jointly dominate during the oxidation reaction. The external diffusion of metal ions reduces the bonding strength of the oxide film, which is easy to cause cracks in the film. The cross-sectional morphology indicates that

the mode of exfoliation for the TiAl alloy is in-film cracking.

### 3.2.3.2 Composition analysis

In order to further investigate the cross-sectional composition of the oxide film, EDS analysis was carried out on the area near this film. Figures 12–15 show the surface scanning results of a cross-section of the TiAl alloy after oxidation at 900 °C for different oxidation times (5, 20, 60, and 100 h, respectively). It can be seen that the oxide film is layered. The outermost layer is  $\text{Al}_2\text{O}_3$ , which is beneficial to the oxidation resistance of the alloy; the sub-outer layer consists of a mixed  $\text{TiO}_2$  and  $\text{Al}_2\text{O}_3$  layer, and the closest layer to the matrix is  $\text{TiO}_2$ .

When the oxidation time is 5 h, the thickness of the oxide layer is small. When the oxidation time is 20 h, the thickness increases, the delamination of the oxide film is more clear. During oxidation, the oxide film exhibits a three-layer structure, with the outermost layer being  $\text{Al}_2\text{O}_3$ . When the oxidation time is 100 h, the oxygen content in the surface scanning area reaches its maximum, 17.30wt.%, and peeling occurs. At the same time, O is mainly distributed outside the oxide film, and the oxide film and oxygen elemental content in the alloy matrix is relatively small. This is because the  $\text{Al}_2\text{O}_3$  in the outermost layer of the alloy matrix is relatively continuous, which hinders, to a certain extent, the diffusion of oxygen into the alloy matrix, and further confirms that the TiAl alloy has a resistance to oxidation at 900 °C.

Figure 16 shows the EDS line scanning results for the TiAl alloy after oxidation at 900 °C for different oxidation times (5,

20, 60, and 100 h). The results indicate that when the oxidation time is 5 h, the O element content in the line scan area is low, at 5.26wt.%. From the oxide film to the substrate, the content of Ti increases firstly, then decreases, and then increases, finally stabilizes. The Al element content shows an initial decrease, and then stabilizes.

The O element content is higher at the outer surface of the oxide film, and decreases in the direction of the substrate. From the changes in element concentrations, it can be seen that Ti and Al continuously diffuse from the interior of the matrix to the outer surface during the high-temperature oxidation process, while O continuously diffuses toward the interior of the alloy matrix. It is precisely due to the continuous diffusion of Ti, Al, and O elements that a stable oxide film is formed. When the oxidation time increases to 100 h, the thickness of the oxide film increases significantly. At the same time, the oxide film is exfoliated, for reasons previously outlined. The outermost layer of the oxide layer is enriched in Al, consisting mainly of  $Al_2O_3$ , and the innermost layer is the Ti-rich layer. There is a clear interface between the oxide film and the substrate. The oxide film may prevent the internal diffusion

of oxygen and reduce the oxidation rate. Meanwhile, the O element content in the matrix is very low, indicating that the alloy has oxidation resistance at this temperature.

### 3.2.4 XPS analysis of oxide film

In order to further determine both the chemical structure of the oxide and the form of its presence, XPS analysis was carried out. Figure 17 shows the full XPS spectrum of the TiAl alloy after different oxidation times (5, 20, 60, and 100 h). It can be seen that after oxidation, the surface of the alloy includes the characteristic peaks of Ti, Al and O, as well as C. However, C was not added during the experiment; its presence in the spectrum is due to surface pollution of the sample [36].

The high-precision XPS scanning maps of Ti 2p, Al 2p and O 1s after different oxidation times at 900 °C for the TiAl alloy are shown in Fig. 18. In the results for 5 h oxidation, as an example, Figs. 18(a)–(c) show that there is a double-state position of Ti 2p, as Ti 2p<sub>3/2</sub> (458.10 eV) and Ti 2p<sub>1/2</sub> (463.68 eV), which is attributed to the Ti-O binding energy in the  $Ti^{4+}$  chemical valence state ( $TiO_2$ ). It is, thus, proven that Ti on the surface of the oxide film exists as  $TiO_2$ . Al 2p also has a double-state

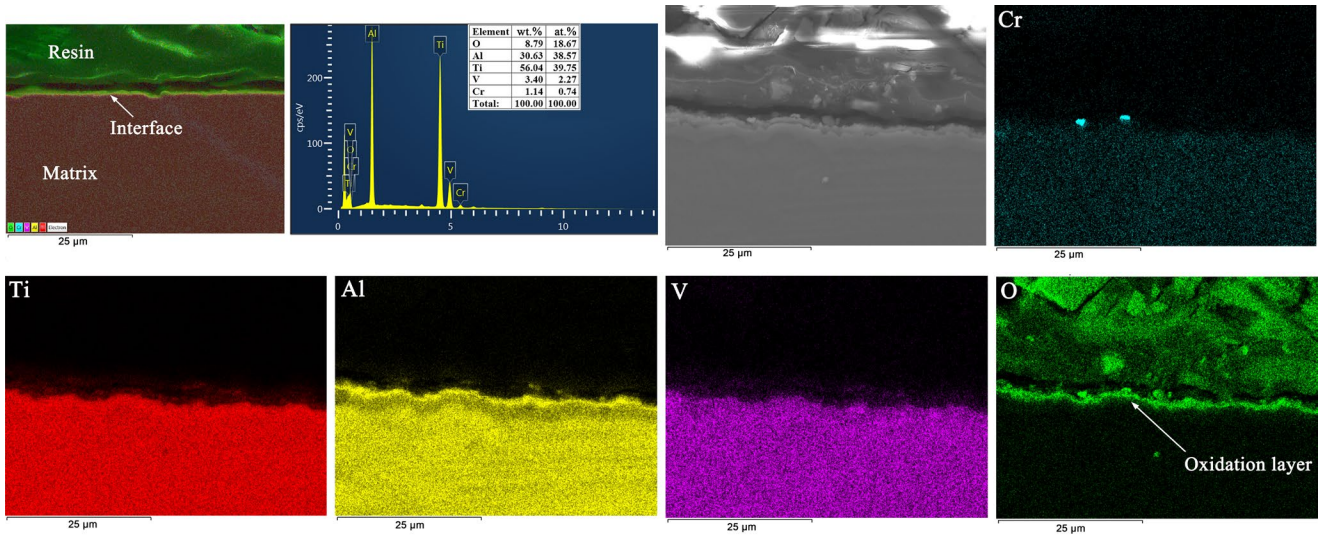


Fig. 12: Surface scanning results of cross-section of TiAl alloy (900 °C/5 h)

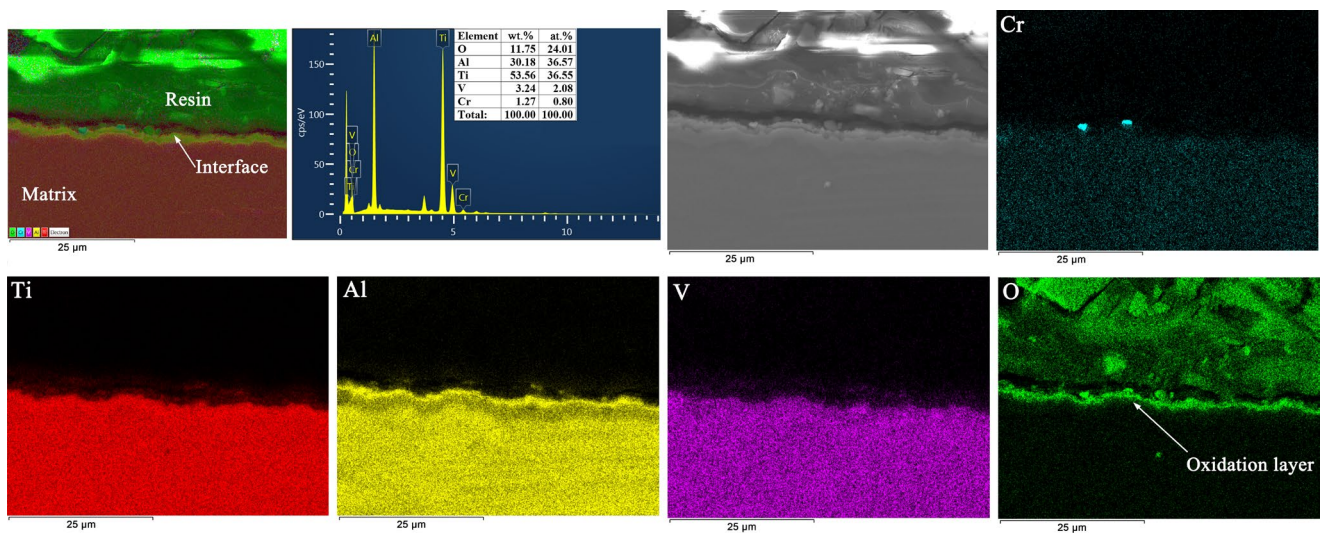


Fig. 13: Surface scanning results of cross-section of TiAl alloy (900 °C/20 h)

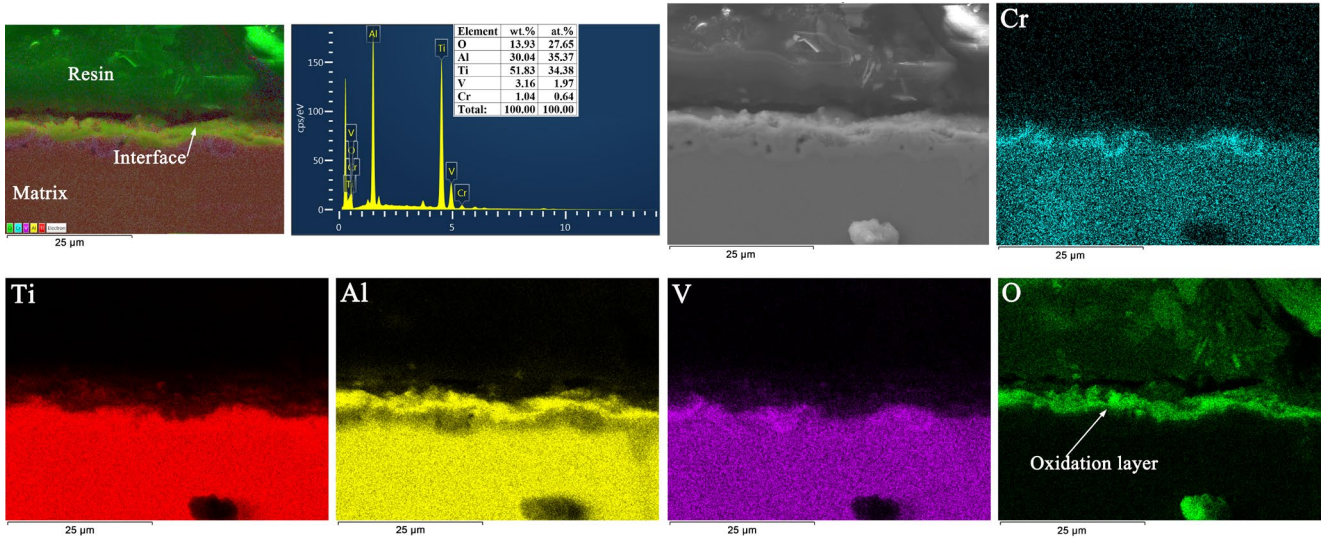


Fig. 14: Surface scanning results of cross-section of TiAl alloy (900 °C/60 h)

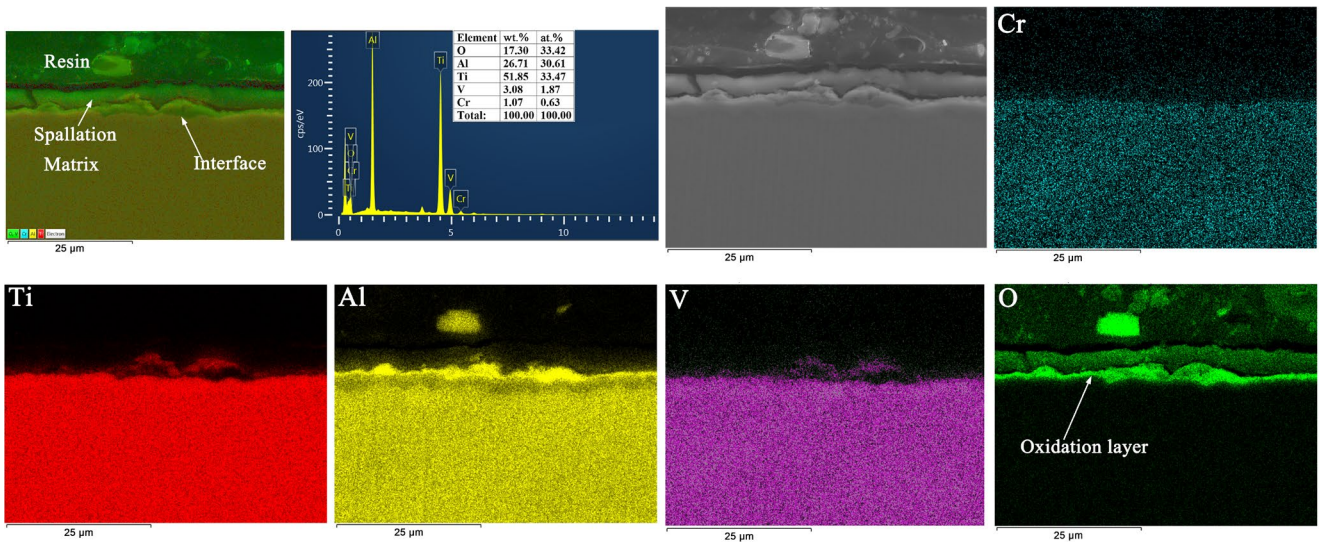


Fig. 15: Surface scanning results of cross-section of TiAl alloy (900 °C/100 h)

position at Al 2p<sub>3/2</sub> (74.38 eV) and Al 2p<sub>1/2</sub> (74.68 eV), where Al exists as Al<sup>3+</sup>, corresponding to the Al-O bond. At the same time, there are two peaks in O 1s. After calibration, the lower binding energy (529.38 eV) corresponds to the chemical valence of O<sup>2-</sup> in TiO<sub>2</sub>, while the higher binding energy (531.18 eV) corresponds to Al<sub>2</sub>O<sub>3</sub>. Figures 18(d)-(l) show that with the increase of oxidation time, the characteristics of XPS spectrum are the same as those of 5 h oxidation. Ti 2p and Al 2p also have a double state position, indicating that the types of surface oxides are the same after oxidation for different time.

Figure 19 shows the XPS spectra of the TiAl alloy after different oxidation times and of the oxide film after etching for 60 s.

For 5 h oxidation time, as an example, it is found that the Ti 2p region shows three dual-state peaks. After calibration, the peak values correspond to the three Ti-O binding energies of Ti<sup>4+</sup> (TiO<sub>2</sub>), Ti<sup>3+</sup> (Ti<sub>2</sub>O<sub>3</sub>) and Ti<sup>2+</sup> (TiO), respectively. The Al 2p region also shows a double-state peak, corresponding to the chemical valence of Al<sup>3+</sup>. At the same time, there are two peaks

in the O 1s region with binding energies of 530.71 eV and 531.56 eV. The higher binding energy corresponds to Al<sub>2</sub>O<sub>3</sub>, and the lower binding energy corresponds to the three titanium oxides with different Ti valences. Figures 19 (d)-(l) show that with the increase of oxidation time, the characteristics of XPS spectrum are the same as those of 5 h oxidation, indicating that the oxide types corresponding to the alloy surface are the same.

To study the elemental distribution at different depths in the oxide film, the relative atomic ratio of each atom (Ti 2p, Al 2p and O 1s) in the oxide film at different depths (different etching times) and different oxidation times was measured, and the results are shown in Table 2. The variation in relative atomic ratio at different etching times and oxidation times is shown in Figs. 20.

Figure 20(a) indicates that the content of Ti atoms increases with the increase of etching time at the same oxidation time. Therefore, the content of titanium oxide increases along the direction from the outer surface of the oxide film toward the substrate. The Al atomic content decreases with increasing

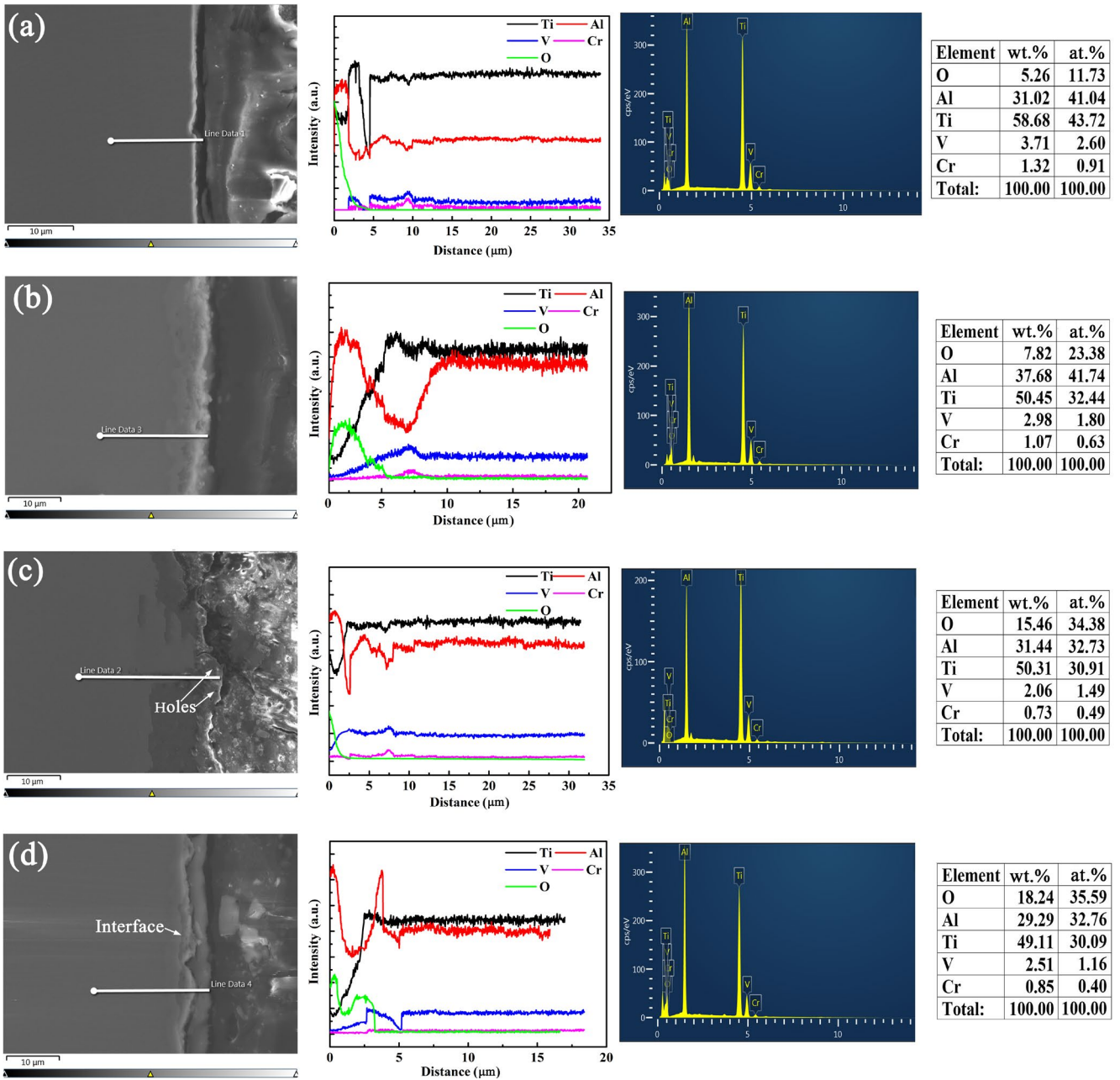


Fig. 16: EDS line scanning results of TiAl alloy at 900 °C: (a) 5 h; (b) 20 h; (c) 60 h; (d) 100 h

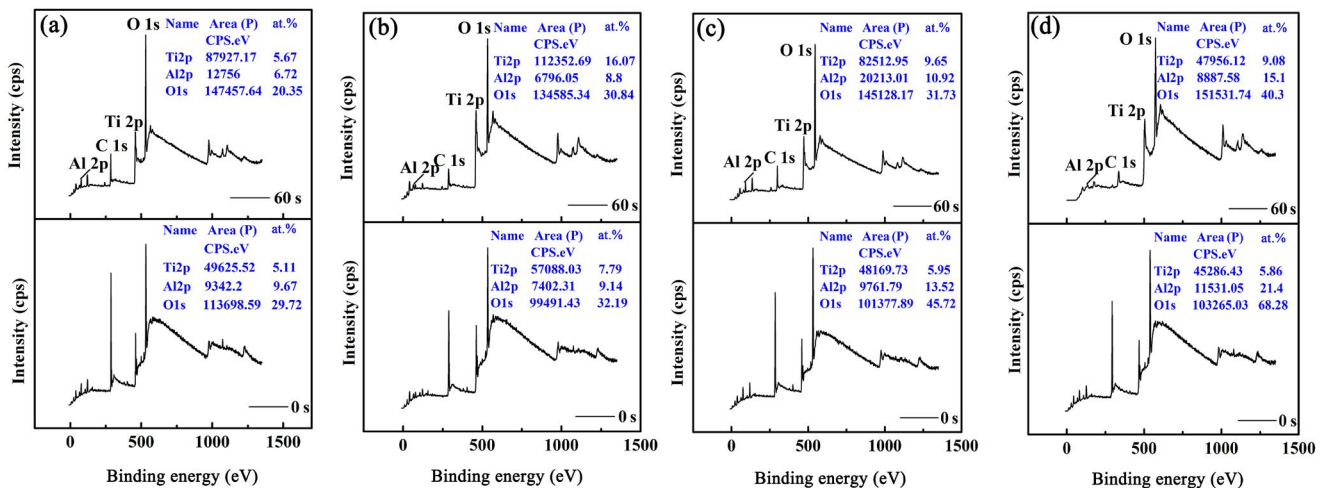


Fig. 17: Full XPS spectrum of TiAl alloy: (a) 5 h; (b) 20 h; (c) 60 h; (d) 100 h

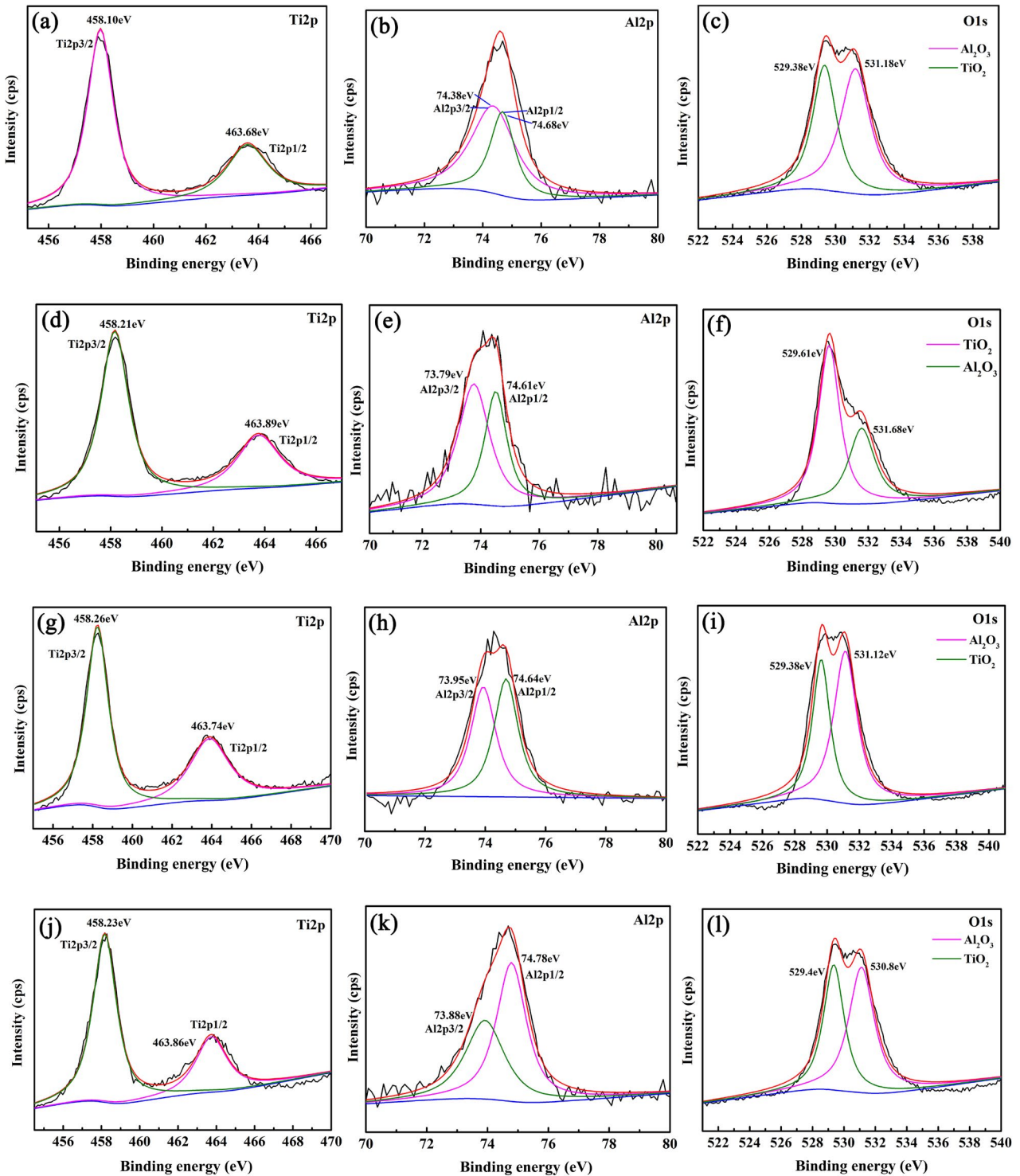


Fig. 18: XPS spectra of TiAl alloy without etching under different oxidation times: (a-c) 5 h; (d-f) 20 h; (g-i) 60 h; (j-l) 100 h

etching time; thus, the aluminum oxide content decreases from the outer surface of the oxide layer toward the matrix. In conclusion, the trend in contents of the two kinds of oxides is obviously opposite.

Figure 20 indicates that, in the oxide film, with increasing oxidation time, the Al and O atomic contents apparently increase with increasing oxidation time, indicating that the oxidation of Al in the alloy is sensitive to changes in oxidation time, consistent with the study of Du et al [37]. High-

temperature oxidation of TiAl is a highly complex physical and chemical process, and the alloy's oxidation resistance depends on the formation and competitive growth of various oxides, such as  $\text{Al}_2\text{O}_3$  and  $\text{TiO}_2$ . After oxidation at different times, an oxide film containing  $\text{Al}_2\text{O}_3$  and  $\text{TiO}_2$  was formed. The oxidation process reaches completion in this system via the dissolution and diffusion of O atoms, resulting in changes in oxide content with both time and sample depth.

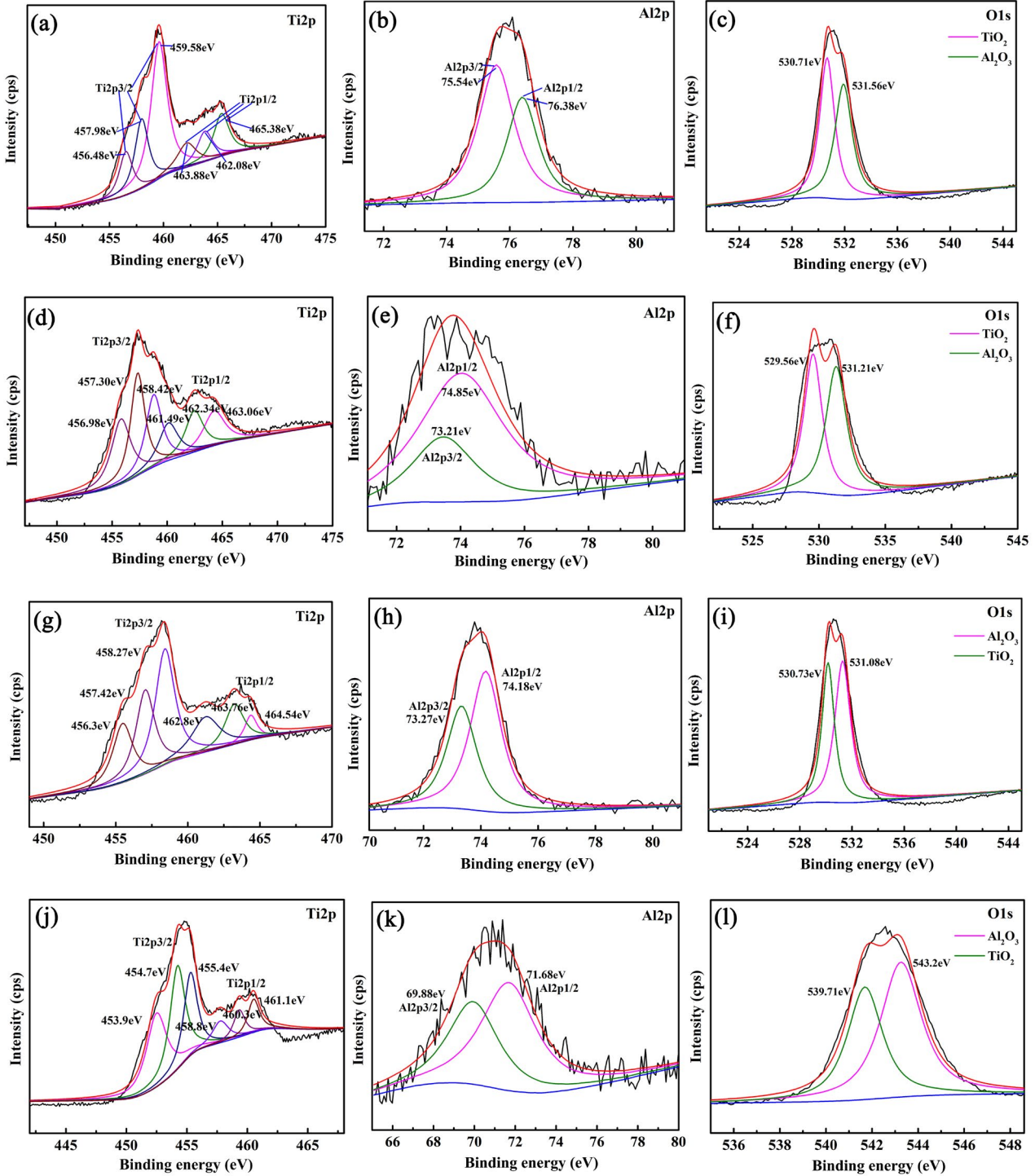


Fig. 19: XPS spectra of TiAl alloy after etching for 60 s under different oxidation times: (a-c) 5 h; (d-f) 20 h; (g-i) 60 h; (j-l) 100 h

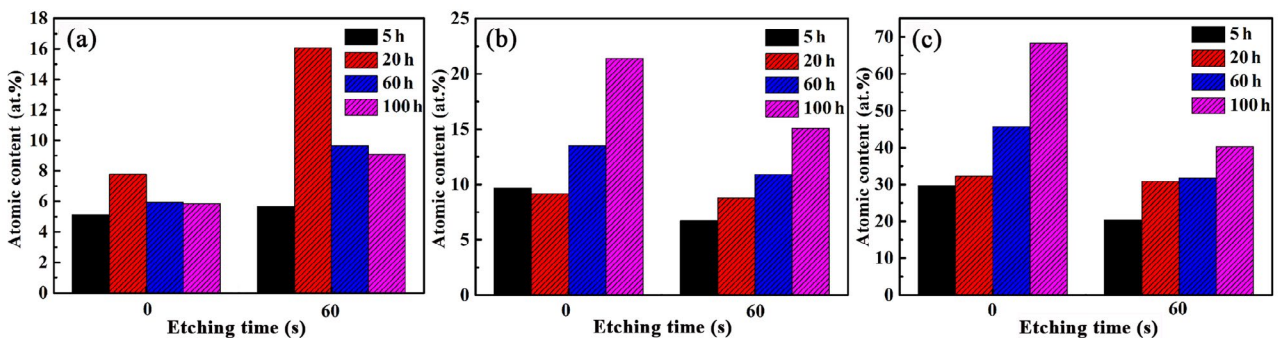


Fig. 20: Relative atomic ratio content at different etching times: (a) Ti 2p; (b) Al 2p; (c) O 1s

**Table 2: Related data of XPS mapping**

Atom	Oxidation time (h)	Etching time (s)	at. %	
Ti 2p	5	0	5.11	
		60	5.67	
	20	0	7.79	
		60	16.07	
	60	0	5.95	
		60	9.65	
	100	0	5.86	
		60	9.08	
	Al 2p	5	0	9.67
			60	6.72
20		0	9.14	
		60	8.80	
60		0	13.52	
		60	10.92	
100		0	21.41	
		60	15.10	
O 1s		5	0	29.72
			60	20.35
	20	0	32.19	
		60	30.84	
	60	0	45.72	
		60	31.73	
	100	0	68.28	
		60	40.32	

## 4 Conclusions

In this work, the oxidation behavior of a TiAl alloy at 900 °C was studied at different oxidation times (5, 20, 60, and 100 h). The conclusions are as follows:

(1) The oxidation kinetics curve approximately obeys the parabolic growth law, and the constant value of the oxidation rate increases with increasing oxidation time.

(2) With the progression of oxidation, Ti and Al atoms continue to diffuse outward, forming TiO<sub>2</sub> and Al<sub>2</sub>O<sub>3</sub> at the surface of the alloy. In the XRD spectrum, the diffraction peak intensity of TiO<sub>2</sub> is significantly higher than that of Al<sub>2</sub>O<sub>3</sub>.

(3) The mismatch of thermal expansion coefficients between the

oxide film and substrate leads to the formation of holes and spalling in the oxide film. The spalling takes the form of intra-film spalling.

(4) The oxide film on the surface of the TiAl alloy shows clear delamination. The TiO<sub>2</sub> content increases from the outer surface of the oxide layer toward the substrate, and the Al<sub>2</sub>O<sub>3</sub> content decreases. The system completes the oxidation process via the dissolution and diffusion of O atoms.

## Acknowledgement

This work was financially supported by the National Natural Science Foundation of China (51805335).

## References

- [1] Ding X F, Zhao Y Q, Zuo J B, et al. Chemical composition analysis on industrial scale ingots and castings of TiAl alloys. *China Foundry*, 2020, 17(6): 441–446.
- [2] Fang H Z, Chen R R, Chen X Y, et al. Microstructure and mechanical properties of Ti44Al6Nb alloys with different cerium contents. *Rare Metals*, 2020, 39(4): 402–407.
- [3] Yang J R, Jiao Z X, Zhu D D, et al. Effects of Ru content on phase transformation and compression property of cast TiAl alloys. *China Foundry*, 2020, 17(6): 393–401.
- [4] Schutze M, Schumacher G, Dettenwanger F, et al. The halogen effect in the oxidation of intermetallic titanium aluminides. *Corrosion Science*, 2002, 44(2): 303–318.
- [5] Szkliniarz A, Moskal G, Szkliniarz W, et al. Improvement of oxidation resistance of Ti-47Al-2W-0.5Si alloy modified by aluminizing method. *Surface & Coatings Technology*, 2015, 277: 270–277.
- [6] Ouyang P X, Mi G B, Li P J, et al. Non-isothermal oxidation behaviors and mechanisms of Ti-Al intermetallic compounds. *Materials*, 2019, 12(13): 2114.
- [7] Zhang S Z, Zhao Y B, Zhang C J, et al. The microstructure, mechanical properties, and oxidation behavior of beta-gamma TiAl alloy with excellent hot workability. *Materials Science & Engineering A*, 2017, 700(17): 366–373.
- [8] Braun R, Kelm K, Froehlich M, et al. Oxidation resistance of γ-TiAl based alloy Ti-45Al-8Nb coated with intermetallic Ti-Al-Cr-Y layers and EB-PVD zirconia topcoats at 950 °C in air. *Surface & Coatings Technology*, 2013, 222: 128–134.
- [9] Yang R, Cui Y Y, Dong L M, et al. Alloy development and shell mould casting of gamma TiAl. *Journal of Materials Processing Technology*, 2003, 135(2–3): 179–188.
- [10] Pflumm R, Donchev A, Mayer S, et al. High-temperature oxidation behavior of multi-phase Mo-containing γ-TiAl-based alloys. *Intermetallics*, 2014, 53: 45–55.
- [11] Pilone D, Felli F, Brotzu A. High temperature oxidation behaviour of TiAl-Cr-Nb-Mo alloys. *Intermetallics*, 2013, 43: 131–137.
- [12] Przybylski K, Prazuch J, Brylewski T, et al. High temperature oxidation behaviour of TiAl8Nb alloy. *Archives of Metallurgy & Materials*, 2013, 58(2): 477–480.
- [13] Wan W J, Han B, Han W, et al. Room-temperature fatigue behavior of TiAl alloy with preferentially oriented lamellar microstructure. *Journal of Iron and Steel Research*, 2017, 29(1): 67–74.

- [14] Zhao X Q, Xu J, Tang L, et al. High temperature oxidation behavior of NiTiNb intermetallic alloys. *Intermetallics*, 2007, 15(8): 1105–1115.
- [15] Liu T L, Lin Y F, Zheng K H, et al. Effect of minor Zr on oxidation resistance and mechanical property of nickel-saving austenitic heat-resistant cast steel. *Materials Research Express*, 2020, 7: 16514.
- [16] Dadé M, Esin V A, Nazé L, et al. Short- and long-term oxidation behaviour of an advanced Ti<sub>2</sub>AlNb alloy. *Corrosion Science*, 2019, 148: 379–387.
- [17] Yao T H, Liu Y, Liu B, et al. Influence of carburization on oxidation behavior of High Nb contained TiAl alloy. *Surface & Coatings Technology*, 2015, 277: 210–215.
- [18] Si J Y, Gao F, Han P B, et al. Simulation on extrusion process of TiAl alloy. *Intermetallics*, 2011, 19(2): 169–174.
- [19] Zhang S Z, Zhao Y B, Zhang C J, et al. The microstructure, mechanical properties, and oxidation behavior of beta-gamma TiAl alloy with excellent hot workability. *Materials Science & Engineering A*, 2017, 700: 366–373.
- [20] Gil A, Hoven H, Wallura E, et al. The effect of microstructure on the oxidation behaviour of TiAl-based intermetallics. *Corrosion Science*, 1993, 34(4): 615–630.
- [21] Teng S J, Liang W, Li Z L, et al. Improvement of high-temperature oxidation resistance of TiAl-based alloy by sol-gel method. *Journal of Alloys & Compounds*, 2008, 464: 452–456.
- [22] Lee D B, Habazaki H, Kawashima A, et al. High temperature oxidation of a Nb-Al-Si coating sputter-deposited on titanium. *Corrosion Science*, 2000, 42(4): 721–729.
- [23] Zhou C G, Yang Y, Gong S K, et al. Effect of Ti-Al-Cr coatings on the high temperature oxidation behavior of TiAl alloys. *Materials Science & Engineering A*, 2001, 307: 182–187.
- [24] Ebach-Stahl A, Eilers C, Laska N, et al. Cyclic oxidation behaviour of the titanium alloys Ti-6242 and Ti-17 with Ti-Al-Cr-Y coatings at 600 and 700 °C in air. *Surface & Coatings Technology*, 2013, 223: 24–31.
- [25] Yang, X, Jiang Z P, Hao G J, et al. Ni-doped Al<sub>2</sub>O<sub>3</sub> coatings prepared by cathode plasma electrolysis deposition on Ti-45Al-8.5Nb alloys. *Applied Surface Science*, 2018, 455: 144–152.
- [26] Wu L K, Wu W Y, Song J L, et al. Enhanced high temperature oxidation resistance for  $\gamma$ -TiAl alloy with electrodeposited SiO<sub>2</sub> film. *Corrosion Science*, 2018, 140: 388–401.
- [27] Wang S Q, Chen K H, Chen L, et al. Effect of Al and Si additions on microstructure and mechanical properties of TiN coatings. *Journal of Central South University*, 2011, 18(2): 310–313.
- [28] Kim D J, Seo D Y, Kim S W, et al. Cyclic oxidation behaviors of TiAl-Nb-Si-based alloys. *Oxidation of Metals*, 2016, 86: 417–430.
- [29] Wei D B, Zhang P Z, Yao Z J, et al. Cyclic oxidation behavior of plasma surface chromising coating on titanium alloy Ti-6Al-4V. *Applied Surface Science*, 2012, 261: 800–806.
- [30] Zhao L L, Li G Y, Zhang L Q, et al. Influence of Y addition on the long time oxidation behaviors of high Nb containing TiAl alloys at 900 °C. *Intermetallics*, 2010, 18: 1586–1596.
- [31] Panov D O, Sokolovsky V S, Stepanov N D, et al. Oxidation resistance and thermal stability of a  $\beta$ -solidified  $\gamma$ -TiAl based alloy after nitrogen ion implantation. *Corrosion Science*, 2020, 177: 109003.
- [32] Swadba R, Nadine L, Peter-Philipp B, et al. Effect of pre-oxidation on cyclic oxidation resistance of  $\gamma$ -TiAl at 900 °C. *Corrosion Science*, 2020, 177: 108985.
- [33] Małecka J, Grzesik W, Hernas A. An investigation on oxidation wear mechanisms of Ti-46Al-7Nb-0.7Cr-0.1Si-0.2Ni intermetallic-based alloys. *Corrosion Science*, 2010, 52(1): 263–272.
- [34] Vojtech D, Čížová H, Jurek K, et al. Influence of silicon on high-temperature cyclic oxidation behaviour of titanium. *Journal of Alloys & Compounds*, 2005, 394(1–2): 240–249.
- [35] Gurrappa I. An oxidation model for predicting the life of titanium alloy components in gas turbine engines. *Journal of Alloys & Compounds*, 2005, 389(1–2): 190–197.
- [36] Maurice V, Despert G, Zanna S, et al. XPS study of the initial stages of oxidation of  $\alpha_2$ -Ti<sub>3</sub>Al and  $\gamma$ -TiAl intermetallic alloys. *Acta Materialia*, 2007, 55(10): 3315–3325.
- [37] Du H L, Datta P K, Lewis D B, et al. High-temperature corrosion of Ti and Ti-6Al-4V alloy. *Oxidation of Metals*, 1996, 45(6): 507–527.